Journal of Alloys and Compounds 514 (2012) 97–102

Contents lists available at SciVerse ScienceDirect

Journal of Alloys and Compounds

journal homepage: www.elsevier.com/locate/jallcom

Structure and luminescence properties of $SrAl_2O_4$:Eu^{2+}, Dy^{3+} by Ba^{2+} and Ca^{2+} co-doping

Wei Xie[a,b,c], Jun Quan[a,c], Haoyi Wu[b], Lexi Shao[a,c], Changwei Zou[a,c], Jun Zhang[a,c], Xiaoyu Shi[a], Yinhai Wang[b,*]

[a] Research Center of Chemistry & Materials Science, Development Center for New Materials Engineering & Technology in Universities of Guangdong, Zhanjiang Normal University, Zhanjiang 524048, People's Republic of China
[b] School of Physics and Optoelectronic Engineering, Guangdong University of Technology, Guangzhou 510006, People's Republic of China
[c] School of Physics Science and Technology, Zhanjiang Normal University, Zhanjiang 524048, People's Republic of China

ARTICLE INFO

Article history:
Received 29 January 2011
Received in revised form 1 November 2011
Accepted 2 November 2011
Available online 18 November 2011

PACS:
61.05.cp
78.20.−e
78.55.Hx
81.15.Gh

Keywords:
Long afterglow phosphor
Solid-state reaction method
X-ray diffraction topography
Optical properties

ABSTRACT

The long afterglow phosphors with Ca and Ba co-doped equally in $Sr_xCa_{(1-x)/2}Ba_{(1-x)/2}Al_2O_4$:$Eu^{2+}$,$Dy^{3+}$ (x = 1.0, 0.8, 0.6, 0.4, 0.2, 0) were synthesized using high temperature solid-state reaction method. X-ray powder diffraction (XRD) patterns show that the crystal phase structure of $SrAl_2O_4$ changes from monoclinic to hexagonal with the decrease of x from 1 to 0.6, and hexagonal $BaAl_2O_4$ and monoclinic $CaAl_2O_4$ coexist when x is 0.2. Nevertheless, when x is reduced to 0, the main phase of sample changes to $BaAl_2O_4$. A blue shift is observed in the emission spectra due to the change in nature of the Eu^{2+} surroundings when x changes from 0.6 to 0. The results given by scanning electronic microscope (SEM) show that phosphors with different structures have similar irregular morphology. The decay characteristics reflect that the phosphors with different structures have different afterglow time. Samples with monoclinic structure have longer afterglow time than samples with hexagonal structure. The measurement of thermoluminescence reveals that the monoclinic structure of the phosphors provides better sites than that of the hexagonal structure for Dy^{3+} ions to generate suitable trap level.

1. Introduction

The long afterglow phosphor can adsorb sunlight, fluorescent lamp or UV light, and store the energy, and then gradually release the energy in the form of persistent luminescence [1–5]. These materials are widely used in many fields [1–3,6], such as emergency signage, power-saving of light sources, the dial plates of glowing watch, and various occasions with lights that glow in the dark. The first long afterglow material is ZnS:Cu, which was discovered in the 18th century. The decay time constant of the afterglow of sulfide is quite short. Since the end of the last century, rare earth ion doping in alkaline earth aluminates have drawn much attention due to their high brightness, better chemical stability, long afterglow and no radicalization [1,4,7]. One of the typical rare earth ions doping in alkaline earth aluminates is $SrAl_2O_4$:Eu^{2+}, Dy^{3+}, which was successfully synthesized by Matsuzawa in 1996 [8]. After that, many researchers have done a lot of works about $SrAl_2O_4$:Eu^{2+},Dy^{3+} because of its high luminescent intensity and long-lasting time [1,4,7,9–11]. Chang et al. reported the effect of B_2O_3 addition on the formation of $SrAl_2O_4$: Eu^{2+},Dy^{3+} phosphor [4]. Xu et al. synthesized single-crystal $SrAl_2O_4$: Eu^{2+},Dy^{3+} nanosheets by a facile two-step method and the as-obtained nanosheets show higher photoluminescence intensity than commercial counterpart [1]. Liu and co-workers investigated the structural, electronic, lattice dynamical, and dielectric properties of $SrAl_2O_4$ within density-function theory [12]. $SrAl_2O_4$: Eu^{2+},Dy^{3+} emits a green light peaking at about 520 nm and shows the long afterglow properties [1,7–11]. It is generally agreed that the Eu^{2+} ions act as luminescence centers in $SrAl_2O_4$: Eu^{2+},Dy^{3+}, and the field strength of the Eu^{2+} surroundings determines the peak positions on the emission spectra [1,7,10,11]. Consequently, Eu^{2+} ions can emit light with varied color in different crystal fields [7,11,13,14].

Recently, Ca or Ba doping in $SrAl_2O_4$: Eu^{2+},Dy^{3+} have been reported [7,13]. In general, the Ca^{2+} ions radius (0.100 nm) is smaller than that of Sr^{2+} ions (0.121 nm), therefore, the lattice parameter of $SrAl_2O_4$ will reduces when the Ca^{2+} replaces the Sr^{2+}. Similarly, when Sr^{2+} is replaced by Ba^{2+} (0.134 nm), the lattice parameter of $SrAl_2O_4$ will increase. These changes in crystal

* Corresponding author. Tel.: +86 20 39322260; fax: +86 20 39322265.
E-mail addresses: carlxw@163.com (L. Shao), xiewei_1984@163.com (Y. Wang).

0925-8388/$ – see front matter © 2011 Elsevier B.V. All rights reserved.
doi:10.1016/j.jallcom.2011.11.048

field have effect on the surroundings of Eu^{2+}, as a result, the controllable optical properties of phosphors can be adjusted by the value of Sr/Ca or Sr/Ba [7,13,14]. However, to the best of our knowledge, the details of the effect resulting from Ca and Ba co-doping in $SrAl_2O_4$: Eu^{2+},Dy^{3+} have not been studied. In this work, we study the $SrAl_2O_4$: Eu^{2+},Dy^{3+} by co-doping Ca^{2+} and Ba^{2+} simultaneously and the Ca^{2+} and Ba^{2+} are doped equally. The $Sr_xCa_{(1-x)/2}Ba_{(1-x)/2}Al_2O_4$:$Eu^{2+}_{0.01}$,$Dy^{3+}_{0.02}$ (x = 1.0, 0.8, 0.6, 0.4, 0.2, 0) phosphor samples are prepared. The crystal phase structures and luminescent properties of phosphors are studied in detail, and the decay characteristics and thermoluminescence properties are also discussed.

2. Experimental details

2.1. Synthesis

The $Sr_xCa_{(1-x)/2}Ba_{(1-x)/2}Al_2O_4$:$Eu^{2+}_{0.01}$,$Dy^{3+}_{0.02}$ (x = 1.0, 0.8, 0.6, 0.4, 0.2, 0) phosphor samples were prepared by the solid-state reaction method. Firstly, according to $Sr_xCa_{(1-x)/2}Ba_{(1-x)/2}Al_2O_4$:$Eu^{2+}_{0.01}$,$Dy^{3+}_{0.02}$, stoichiometric composition of $SrCO_3$, $BaCO_3$, $CaCO_3$, Al_2O_3, Eu_2O_3, and Dy_2O_3 were mixed and milled thoroughly in agate mortar for 2 h. All of these materials were analytical purity. 10 mol% of H_3BO_3 was added as flux. Secondly, well-mixed powders were sintered at 1350 °C for 4 h with a weak reducing atmosphere of flowing 5%H_2 + 95%N_2. Finally, the phosphor samples $SrAl_2O_4$:$Eu^{2+}_{0.01}$,$Dy^{3+}_{0.02}$(SAM1), $Sr_{0.8}Ca_{0.1}Ba_{0.1}Al_2O_4$:$Eu^{2+}_{0.01}$,$Dy^{3+}_{0.02}$ (SAM2), $Sr_{0.6}Ca_{0.2}Ba_{0.2}Al_2O_4$:$Eu^{2+}_{0.01}$,$Dy^{3+}_{0.02}$ (SAM3), $Sr_{0.4}Ca_{0.3}Ba_{0.3}Al_2O_4$:$Eu^{2+}_{0.01}$,$Dy^{3+}_{0.02}$ (SAM4), $Sr_{0.2}Ca_{0.4}Ba_{0.4}Al_2O_4$:$Eu^{2+}_{0.01}$,$Dy^{3+}_{0.02}$ (SAM5), $Ca_{0.5}Ba_{0.5}Al_2O_4$:$Eu^{2+}_{0.01}$,$Dy^{3+}_{0.02}$ (SAM6) were obtained, respectively.

2.2. Measurement

The phase identification of the samples was carried out by X-ray powder diffraction (XRD) using a diffractometer with Cu Kα irradiation (λ = 1.5406 Å) at 36 kV tube voltage and 20 mA tube current at room temperature. The SEM analysis was conducted on Philips XL-30 Scanning Electron Microscope. The photoluminescence (PL) excitation and emission spectra were taken on a Hitachi F-7000 fluorescence spectrophotometer. The emission spectra were scanned in the range of wavelengths from 400 to 600 nm, and each sample was loaded into a circular holder and excited with 360 nm radiation from a pulsed xenon lamp. The decay curves were recorded by GFZF-2A single-photon counter system. Prior to the decay curve measurements, the phosphors were excited by UV light for 3 min. The thermoluminescence (TL) curves were measured using a FJ427A1 thermoluminescent dosimeter. All the samples were excited by UV for 1 min.

3. Results and discussion

3.1. XRD phase analysis

In order to determine the crystalline structure, XRD analysis was carried out. Fig. 1 shows the XRD patterns of all the phosphors. Patterns given in Fig. 1(a) and (b) show that SAM1 and SAM2 are pure single-phase compounds, and take accordance with the JCPDS data file (No. 34-0379). All of the diffraction peaks come from the monoclinic-phase $SrAl_2O_4$ (space group $P2_1$), and no other phases are observed. Compared SAM1 with SAM2, it indicates that there is no peak shift in the diffraction patterns; this implies that the lattice structure does not change obviously in the two samples.

The diffraction peaks in Fig. 1(c) can be indexed to the hexagonal phase structure of $SrAl_2O_4$ (No. 31-1336, space group $P6_322$), and no other phase is detected. In general, $SrAl_2O_4$ undergoes a phase transformation from monoclinic to hexagonal structure at 950 K [15], so the hexagonal structure of $SrAl_2O_4$ just exists over 950 K. Seeing from Fig. 1(a) and (c), it is obvious that the phase transformation of $SrAl_2O_4$ occurs when the ratio Sr:Ba:Ca is 0.6:0.2:0.2. The diffraction pattern of SAM3 is measured at room temperature and the JCPDS standard file (No. 31-1336) is measured by high temperature X-ray diffraction analysis (above 950 K). Thus, the high temperature phase of $SrAl_2O_4$ was obtained at room temperature by Ca^{2+} and Ba^{2+} ions co-doped for the first time. Comparing Fig. 1(c) with JCPDS standard file (No. 31-1336), one finds a fine

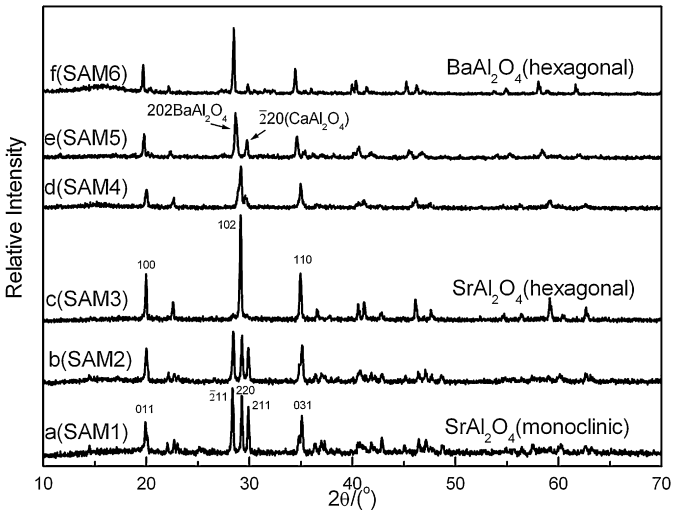

Fig. 1. The XRD patterns of the phosphors samples (SAM1: Sr:Ca:Ba = 1:0:0, SAM2: Sr:Ca:Ba = 0.8: 0.1:0.1, SAM3: Sr:Ca:Ba = 0.6: 0.2:0.2, SAM4: Sr:Ca:Ba = 0.4: 0.3:0.3, SAM5: Sr:Ca:Ba = 0.2: 0.4:0.4, SAM6: Sr:Ca:Ba = 0:0.5:0.5).

distinction in high angles due to the decrease of the parameter of the crystal lattice at the lower temperature.

The hexagonal phase structure $SrAl_2O_4$ is also found in SAM4 (see Fig. 1(d)) with a minor content of $BaAl_2O_4$ (No. 17-0306) phase and a little $CaAl_2O_4$ (No. 23-1036) phase. As the ratio Sr:Ba:Ca is 0.4:0.3:0.3 in SAM4, the Sr^{2+} ions tend to replace the Ca^{2+} and Ba^{2+} ions in the $CaAl_2O_4$ and $BaAl_2O_4$ phase, respectively. However, the ionic radius of Sr^{2+} (0.121 nm) is greater than that of Ca^{2+} (0.100 nm), the replacement of Ca^{2+} by Sr^{2+} will lead to the increase of the lattice parameter of $CaAl_2O_4$ structure, and interplanar crystal spacing d will becomes larger. According to Bragg equation, namely $2d\sin\theta = \lambda$ with λ, θ representing the wavelength of the X-ray and the incident angle, respectively. Comparing SAM4 with the JCPDS standard data file (No. 23-1036), one finds the diffraction peaks of $CaAl_2O_4$ shift to a lower angles due to the replacement of Ca^{2+} (0.100 nm) by Sr^{2+} (0.121 nm) in SAM4, but the result of $BaAl_2O_4$ is opposite to that of $CaAl_2O_4$.

Fig. 1(e) and (f) reflect that the $SrAl_2O_4$ phase cannot be found in SAM5 and SAM6 while the $CaAl_2O_4$ and $BaAl_2O_4$ are obviously coexisted. The $BaAl_2O_4$ phase can be formed easily at lower temperature because the ionization energy of Ba is lower than that of Ca, and the $BaAl_2O_4$ phase is generated at the beginning of the sample preparation process. In Ref. [16], the $CaAl_2O_4$ phase will be generated if the Ba:Ca ratio is higher than 0.6:0.4 in the raw materials. In this study, the Ca^{2+} and Ba^{2+} are doped equally, so $CaAl_2O_4$ phase exists in SAM5 and SAM6, respectively. As the Sr:Ba:Ca ratio is 0.2:0.4:0.4 in SAM5, it may coexist that Sr^{2+} ions replace the Ca^{2+} (Ba^{2+}) ions in the $CaAl_2O_4$ ($BaAl_2O_4$) phase, so a visible shift in SAM5 can be observed.

In SAM6, the ratio of Sr, Ba and Ca is 0:0.5:0.5, so the replacement of Ca^{2+} and Ba^{2+} may increase (reduce) the lattice parameter of $CaAl_2O_4$($BaAl_2O_4$) phase, then a tiny shift can be observed in the diffraction peaks, as shown in Fig. 1(f). One can also finds that the major phase is hexagonal $BaAl_2O_4$ in SAM6 due to the lower synthesis temperature of $BaAl_2O_4$.

When x reduces from 1 to 0.6, the phases of samples change from the monoclinic $SrAl_2O_4$ to hexagonal $SrAl_2O_4$, furthermore x reduces to 0.2, the hexagonal $BaAl_2O_4$ (17-0306) and monoclinic $CaAl_2O_4$ coexist. Nevertheless, when x reduces to 0, the major phase is $BaAl_2O_4$. Obviously, the crystal structure of phosphors is changed with the increase of Ca^{2+} and Ba^{2+} ions. The major phase of SAM1 and SAM2 belongs to monoclinic structure, while the main

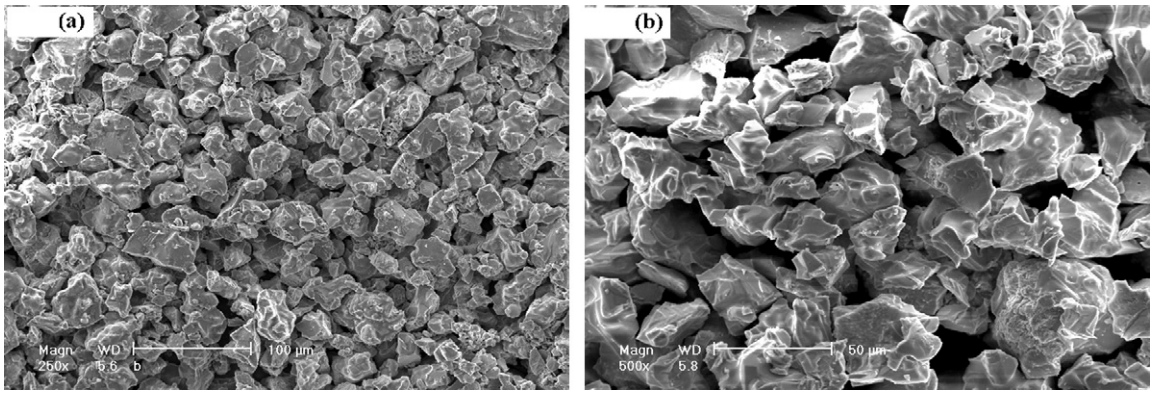

Fig. 2. The SEM photos of SAM2 and SAM4((a) for SAM2 and (b) for SAM4).

components of SAM3, SAM4, SAM5 and SAM6 belongs to hexagonal structure.

3.2. Morphology of phosphors

The SEM study was carried out to investigate the surfaces morphology and the crystallite size of the synthesized phosphor powders. Fig. 2(a) and (b) show the SEM micrographs for SAM2 and SAM4, respectively. Obviously, both samples have similar irregular morphology with angularity and corners, and the grain sizes varied from several to tens microns. The influence of growth way of different crystal structures on morphology was covered with the solid state reaction [17], and various ions doped have very little influence on the grain sizes and morphology of phosphors.

3.3. Spectra analysis

In order to study the luminescent properties, the excitation and emission spectra of all the samples were recorded. In Fig. 3, the excitation spectra of SAM1, SAM2 and SAM3 exhibit a broad band nearly from 270 to 450 nm, which corresponds to the crystal field splitting of the Eu^{2+} 5d orbital. The $4f^7(^8S)$–$4f^65d^1$ transition of Eu^{2+} is strongly depended on the crystal field symmetry of the host lattice, so it causes the splitting of the excited state involving 5d orbital. In SAM1, SAM2 and SAM3, the influence of the variation of chemical composition on the excitation spectra is not evident. Fig. 3(e)–(g) show the excitation spectra of SAM3, SAM4 and SAM5 monitored at different emit wavelength. All the three compositions show broad excitation spectra with different excitation maxima. The results of excitation spectra show that all the samples could be excited by ultraviolet and visible light.

Fig. 4 shows the emission spectra of the phosphor samples under a 360 nm excitation. SAM1 (Fig. 4(a)) and SAM2 (Fig. 4(b)) exhibit a broad blue–green (For interpretation of the references to color in this text, the reader is referred to the web version of the article.) emission band peaking at 515 nm due to the 5d–4f transition of Eu^{2+}ions, and the result is similar to previous reports of $SrAl_2O_4$:Eu^{2+} [9,10]. What is more, the positions of two emission peaks in the phosphorescence do not change with a low amount of the Ca^{2+} ions and Ba^{2+} ions doping.

When x is reduced to 0.6, SAM3 exhibits a broad blue–green emission band with peak at 507 nm, it can be attributed to $4f^65d^1 \leftrightarrow 4f^7(^8S)$ transition position of Eu^{2+} being strongly dependent on the crystal field strength of the host lattice and splitting of $4f^65d^1$ being dependent on symmetry of the host lattice [18,19]. By the analysis of two-peaks fitting, the emission spectra of the SAM4, SAM5 and SAM6 are shown in Table 1. There are different ions replacements in SAM4, SAM5 and SAM6. When the foreign atom is introduced to an interstitial site, this will be accompanied by the distortion in the host lattice. The distortion arises from a size mismatch between the doped and the substituted ions in the host matrix [20]. In the case of SAM4, SAM5 and SAM6, an anamorphic crystal lattices will result, when the surroundings of Eu^{2+} ions

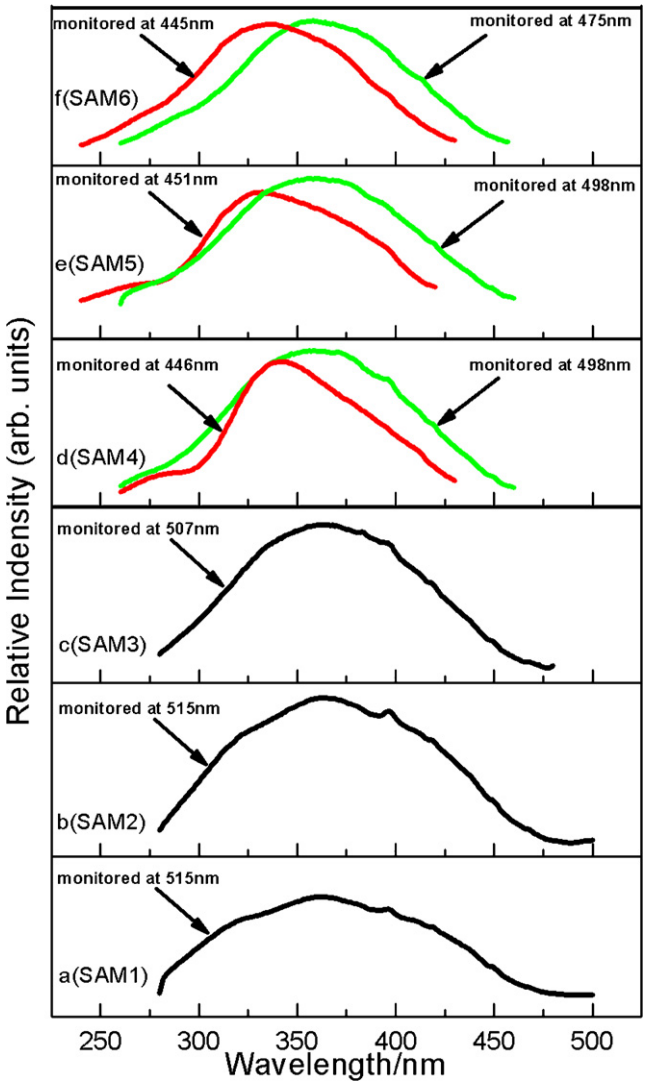

Fig. 3. The excitation spectra of the phosphors monitored at different wavelength (SAM1: Sr:Ca:Ba = 1:0:0, SAM2: Sr:Ca:Ba = 0.8: 0.1:0.1, SAM3: Sr:Ca:Ba = 0.6: 0.2:0.2, SAM4: Sr:Ca:Ba = 0.4: 0.3:0.3, SAM5: Sr:Ca:Ba = 0.2: 0.4:0.4, SAM6: Sr:Ca:Ba = 0:0.5:0.5).

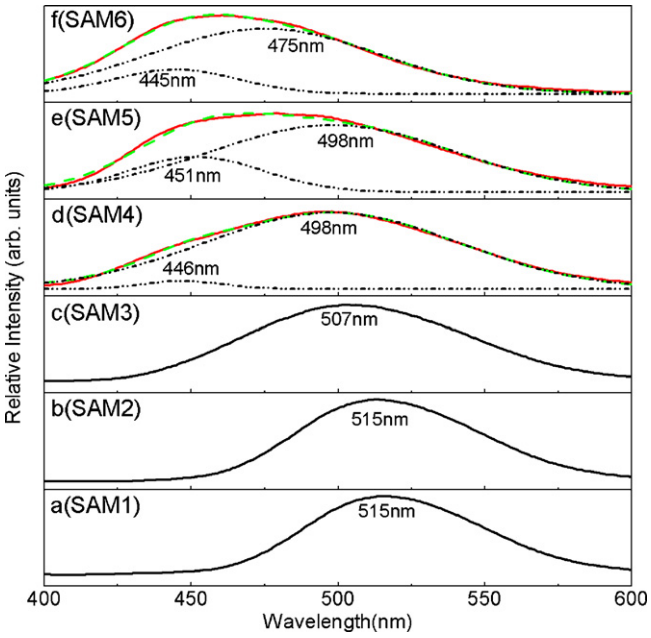

Fig. 4. The emission spectra of the phosphors (SAM1: Sr:Ca:Ba = 1:0:0, SAM2: Sr:Ca:Ba = 0.8: 0.1:0.1, SAM3: Sr:Ca:Ba = 0.6: 0.2:0.2, SAM4: Sr:Ca:Ba = 0.4: 0.3:0.3, SAM5: Sr:Ca:Ba = 0.2: 0.4:0.4, SAM6: Sr:Ca:Ba = 0:0.5:0.5).

Table 1
Peaks of emission spectra of SAM4, SAM5 and SAM6 by two-peaks fitting.

Samples	Substrate		
	$SrAl_2O_4$ (nm)	$CaAl_2O_4$ (nm)	$BaAl_2O_4$ (nm)
SAM4	498	446	
SAM5		451	498
SAM6		445	475

is changed and thus the emission and excitation characteristics do not match with pure phases reported by other researchers shown in Table 2 [7,16,21]. Moreover, the emission characteristics of $CaAl_2O_4$ are also reflecting as weak emission in Fig. 4, and predominant emission can be attributed to phases of $SrAl_2O_4$ and $BaAl_2O_4$.

SAM1 and SAM2 are still monoclinic when the Ca^{2+} ions and Ba^{2+} ions are doped in the low content, and no obvious change can be observed in the luminescence of Eu^{2+}ions. The different replacements in SAM4, SAM5 and SAM6 result to the alterations of the crystal structure, so the luminescent wavelength of Eu^{2+}ions is changed. The emission colors of these samples changed from blue–green to blue. In other words, the emission light colors of the hexagonal structure phosphor samples can be adjusted by the content of Ba^{2+} and Ca^{2+} ions.

3.4. Decay characteristics

The decay curves of the phosphors are recorded after 3 min irradiation of UV light. In order to illustrate the decay characteristics with different host structure, we compare the curve of SAM1 to the curve of SAM5, as shown in the Fig. 5. Both the decay

Table 2
Reported results for pure phases from Refs. [6,9,13].

Number of Refs.	Pure phases		
	$SrAl_2O_4$ (nm)	$CaAl_2O_4$ (nm)	$BaAl_2O_4$ (nm)
Ref. [7]	517	443	
Ref. [16]		430	500
Ref. [20]		430	

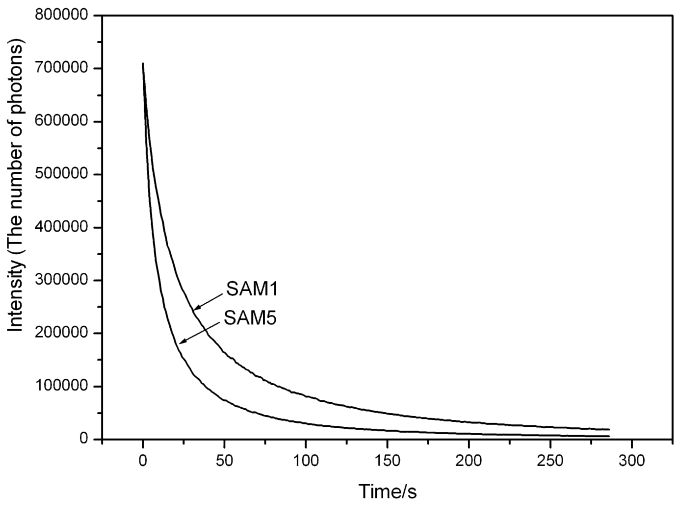

Fig. 5. The decay curves of SAM1 and SAM5 with the equal beginning intensity.

processes contain a rapid-decaying process and a slow-decaying one. The afterglow characteristics were evaluated utilizing curve fitting as referred to Refs. [22–25]. The decay curves are fitted using double exponential equation:

$$I = I_1 \exp\left(\frac{-t}{\tau_1}\right) + I_2 \exp\left(\frac{-t}{\tau_2}\right), \quad (1)$$

where I represents the phosphorescent intensity; I_1 and I_2 are two constants; t represents the time; τ_1 and τ_2 are decay constants which decide the decay rate for the rapid and the slow exponentially decay components. The fitting results of the parameters of τ_1 and τ_2 are listed in Table 3, and the fitting curves are shown in Fig. 6. From the profiles in Fig. 6, one can finds both rapid-decaying parameter τ_1 and slow-decaying parameter τ_2 of SAM1 are greater than that of SAM5. This result reflects that phosphors with monoclinic structure show better afterglow characteristics than phosphor with hexagonal structure, for the reason that the monoclinic structure provides better crystal field surroundings than hexagonal structure. We contend that phosphors with different host structures show different decay characteristics, and in our specimen, the samples with monoclinic structure have longer afterglow time than samples with hexagonal structure.

3.5. Thermoluminescence

In order to make a further research about the decay characteristics and trap level, the TL of SAM1 and SAM5 were detected and the curves are shown in Fig. 7. Thermoluminescence glow curves were measured using a FJ-427Al thermoluminescent dosimeter by heating the irradiated samples from room temperatures to 200 °C. The detector in FJ-427A1 thermoluminescent dosimeter is photomultiplier. The response time of the photomultiplier is 20 ns, and the spectral response is in the range of 300–650 nm. The samples were excited by UV for 1 min and the measurement started 15 min after switching off the excitation source. The heating rate is 1 K/s. The samples were measured for three times, and the averaged data was used in Fig. 7. The detections above were operated at room temperature. In order to exhibit long afterglow at room temperature,

Table 3
Fitting results for SAM1 and SAM5.

Samples	τ_1 (s)	τ_2 (s)
SAM1	16.38	100.94
SAM5	8.24	58.33

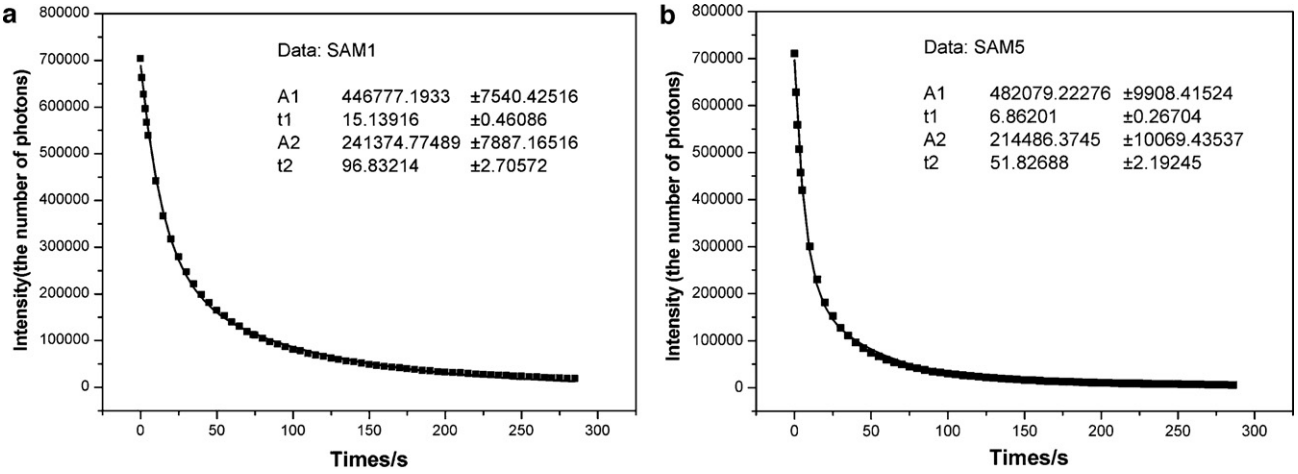

Fig. 6. The fitting curves of SAM1 and SAM5.

the phosphor should have suitable trap level and trap density, and the trap is generated by the doping rare earth RE^{3+}ions (RE = Dy, Nd and La, etc.). If the trap energy level is deeper and the number of the holes is larger, the afterglow time will become longer. However, the trap energy level should not be too deep, because the energy maybe too high to obtain by thermal agitation at room temperature and the afterglow cannot occur. On the other hand, if the depths of the trap levels are too shallow, the phosphor would show rapid decay process and the phosphorescence would not last for a long time. The depth of the trap levels could be estimated by TL glow curves (in Fig. 7) fitted by a general order kinetics formula [3,26,27]. The TL intensity as a function of temperature, T, is as follows:

$$I(T) = sn_0 \exp\left(-\frac{E_t}{k_B T}\right) \times \left[\frac{(l-1)s}{\beta} \times \int_{T_0}^{T} \exp\left(-\frac{E_t}{K_B T}\right) dT + 1\right]^{-l(l-1)}, \quad (2)$$

where n_0 is the concentration of trapped charges at $T = 0$, k_B is the Boltzmann's constant, β the heating rate, E_t the activation energy (or depth of the trap), s the frequency factor and l the order of kinetics. Parameters E_t and n_0 are the most important parameters that describe the physical properties of the traps generated by the auxiliary activators. In fact, trap level depth E_t is proportional to one corresponding glow peak temperature, the afterglow duration of the phosphor is also proportional to the trap density n_0, and the intensity of glow peaks is proportional to n_0. As the effect of s on

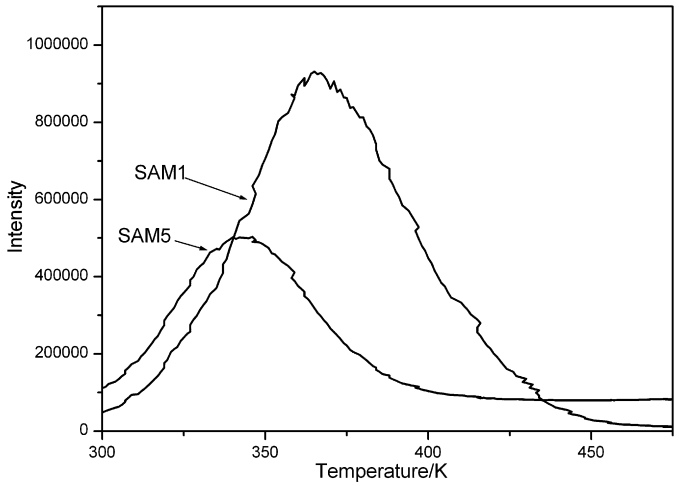

Fig. 7. The thermoluminescence curves of SAM1 and SAM5.

Table 4
T_m and trap depth E_t of SAM1 and SAM5.

Samples	FWHM	T_m (K)	Trap depth (eV)
SAM1	60	369	0.738
SAM5	55	344	0.688

T_m is neglected and the frequency of an electron escaping the trap is assumed as $1/s$, the thermal activation energy or the trap depth E_t (eV) could be estimated by $E_t = T_m/500$ [28–30], where T_m (K) is the glow peak temperature in the TL curve (all data are listed in Table 3), the unit of constant is 500 K/eV.

In Table 4, the trap in SAM1 (0.738 eV) is deeper than that of SAM5 (0.688 eV), and it reflects that the trap generated by Dy^{3+}ions in monoclinic structure phosphor is deeper than that of hexagonal structure. Meanwhile, the full widths at half maximum (FWHM) of SAM1 and SAM5 show a little difference, it indicates that there may be two different kinds of traps due to the two different structure phosphors. Although there are different traps exist in hexagonal structure phosphors by Ca^{2+} and Ba^{2+} co-doping, the afterglow duration of hexagonal structure phosphors are also shorter than that of monoclinic structure phosphors. Concludly, the phosphor in monoclinic structure provides Dy^{3+}ions with better sites than that of the phosphor with hexagonal structure to generate suitable trap level to catch the holes, which are generated by Eu^{2+} in ground 4f.

4. Conclusions

The long afterglow phosphors with Ca^{2+} and Ba^{2+} ions co-doped equally in the $Sr_xCa_{(1-x)/2}Ba_{(1-x)/2}Al_2O_4:Eu^{2+}, Dy^{3+}$ ($x = 1.0, 0.8, 0.6, 0.4, 0.2, 0$) were synthesized successfully by solid-state reaction method. With the increase of Ca^{2+} and Ba^{2+}, the structure of the phosphors changes from the monoclinic to hexagonal. Especially, we found that when Sr:Ba:Ca = 0.6:0.2:0.2, hexagonal structure $SrAl_2O_4$ (31-1336) was generated at room temperature. SEM photos reveal that phosphors with different structures show similar irregular morphology. A blue shift was observed in the emission spectra when x reduce from 0.6 to 0. Decay curves reflect that afterglow time of phosphors with monoclinic structure is longer than that of the phosphor in the hexagonal structure. TL measurements show that the trap generated by Dy^{3+}ions in monoclinic structure phosphor is deeper than that in hexagonal structure. We can draw a conclusion that monoclinic structure provides better sites for Dy^{3+}ions to generate suitable trap level to catch the holes generated by Eu^{2+} than that of the hexagonal structure.

Acknowledgements

This work is supported by the National Natural Science Foundation of China (Nos 20871033 and 61106124), Natural Science Foundation of Guangdong Province (No. S2011040002130) and Natural Science Fundation of Zhanjiang Normal University (No. QL1020).

References

[1] Y.F. Xu, D.K. Ma, M.L. Guan, X.A. Chen, Q.Q. Pan, S.M. Huang, J. Alloys Compd. 502 (2010) 38.
[2] H.Y. Wu, Y.H. Hu, L. Chen, X.J. Wang, J. Alloys Compd. 509 (2011) 4304.
[3] C.J. Fu, Y.H. Hu, Y.H. Wang, H.Y. Wu, X.J. Wang, J. Alloys Compd. 502 (2010) 423.
[4] Y.L. Chang, H.I. Hsiang, M.T. Liang, J. Alloys Compd. 461 (2008) 598.
[5] T.K. Ji, H.Y. Jiang, F. Chen, J. Alloys Compd. 502 (2010) 180.
[6] D. Jia, X.J. Wang, E. van der Kolk, W.M. Yen, Opt. Commun. 204 (2002) 247.
[7] C. Liu, Y.H. Wang, Y.H. Hu, R. Chen, F. Liao, J. Alloys Compd. 470 (2009) 473.
[8] T. Matsuzawa, Y. Aoki, N. Takeuchi, Y. Murayama, J. Electrochem. Soc. 143 (8) (1996) 2670.
[9] T. Katsumata, T. Nabae, K. Sasajima, T. Matsuzawa, J. Cryst. Growth 183 (1998) 361.
[10] Y.Q. Lu, Y.X. Li, Y.H. Xiong, D. Wang, Q.G. Yin, Microelectron. J. 35 (2004) 379.
[11] K.S. Bartwal, H. Ryu, M.G. Brik, I. Sildos, Opt. Mater. 32 (2010) 1329.
[12] B. Liu, M. Gu, X.L. Liu, S. Huang, C. Ni, J. Alloys Compd. 509 (2011) 4300.
[13] H. Ryu, B.K. Singh, K.S. Bartwal, Physica B 403 (2008) 126.
[14] Q.L. Wu, Z. Liu, H. Jiao, Physica B 404 (2009) 2499.
[15] C.M.B. Henderson, D. Taylor, Miner. Mag. 45 (1982) 111.
[16] S.H. Ju, U.S. Oh, J.C. Choi, H.L. Park, T.W. Kim, C.D. Kim, Mater. Res. Bull. 35 (2000) 1831.
[17] Z.C. Wu, J.X. Shi, J. Wang, H. Wu, Q. Su, M.L. Gong, Mater. Lett. 60 (2006) 3499.
[18] P. Dorenbos, J. Lumin. 128 (2008) 578.
[19] P. Dorenbos, J. Electrochem. Soc. 152 (7) (2005) H107.
[20] K. Srinivasa Rao, R. Balasubramaniam, Int. J. Hydrogen Energy 21 (7) (1996) 563.
[21] S. Tanaka, I. Ozaki, T. Kunimoto, K. Ohmi, H. Kobayashi, J. Lumin. 87–89 (2000) 1250.
[22] R. Chen, Y.H. Wang, Y.H. Hu, Z.F. Hu, C. Liu, J. Lumin. 128 (2008) 1180.
[23] R. Sakai, T. Katsumata, S. Komuro, T. Morikawa, J. Lumin. 85 (1999) 149.
[24] Z.X. Yuan, C.K. Chang, D.L. Mao, W.J. Ying, J. Alloys Compd. 377 (2004) 268.
[25] H. Kubo, H. Aizawa, T. Katsumata, S. Komuro, T. Morikawa, J. Cryst. Growth 275 (2005) 1767.
[26] T. Katsumata, S. Toyomane, A. Tonegawa, Y. Kanai, U. Kaneyama, J. Cryst. Growth 237–239 (2002) 361.
[27] H.Y. Wu, Y.H. Hu, Y.H. Wang, B.D. Zeng, Z.F. Mou, L.Y. Deng, W. Xie, J. Alloys Compd. 486 (2009) 549.
[28] S.W.S. McKeever, Thermoluminescence of Solids, Cambridge University Press, Cambridge, 1985, p. 99.
[29] C.S. Shalgaonkar, A.V. Narlikar, J. Mater. Sci. 7 (1972) 1465.
[30] C.F. Guo, Q. Tang, C.X. Zhang, D.X. Huang, Q. Su, J. Lumin. 126 (2008) 333.